RESEARCH ARTICLE | MAY 03 2021

Topological constraints in the reconnection of vortex braids

S. Candelaresi ✉; G. Hornig; B. Podger; ... et. al

Physics of Fluids 33, 056101 (2021)
https://doi.org/10.1063/5.0047033

Physics of Fluids ARTICLE scitation.org/journal/phf

Topological constraints in the reconnection of vortex braids

Cite as: Phys. Fluids 33, 056101 (2021); doi: 10.1063/5.0047033
Submitted: 9 February 2021 · Accepted: 8 April 2021 ·
Published Online: 3 May 2021

View Online Export Citation CrossMark

S. Candelaresi,[1,2,a] G. Hornig,[2] B. Podger,[2] and D. I. Pontin[2,3]

AFFILIATIONS

[1]School of Mathematics and Statistics, University of Glasgow, Glasgow G12 8QQ, United Kingdom
[2]Division of Mathematics, University of Dundee, Dundee DD1 4HN, United Kingdom
[3]School of Mathematical and Physical Sciences, University of Newcastle, Callaghan, NSW 2308, Australia

[a]Author to whom correspondence should be addressed: simon.candelaresi@gmail.com

ABSTRACT

We study the relaxation of a topologically nontrivial vortex braid with zero net helicity in a barotropic fluid. The aim is to investigate the extent to which the topology of the vorticity field—characterized by braided vorticity field lines—determines the dynamics, particularly the asymptotic behavior under vortex reconnection in evolution at high Reynolds numbers (25 000). Analogous to the evolution of braided magnetic fields in plasma, we find that the relaxation of our vortex braid leads to a simplification of the topology into large-scale regions of opposite swirl, consistent with an inverse cascade of the helicity. The change of topology is facilitated by a cascade of vortex reconnection events. During this process, the existence of regions of positive and negative kinetic helicities imposes a lower bound for the kinetic energy. For the enstrophy, we derive analytically a lower bound given by the presence of unsigned kinetic helicity, which we confirm in our numerical experiments.

I. INTRODUCTION

It is well established that the degree of tangling/knottedness of vorticity field lines can have important implications for the dynamics of a fluid.[1,2] In a barotropic fluid in the ideal case with zero viscosity this tangling is preserved, restricting the lowest energy state to which the fluid has access. This has been demonstrated both in experiments[3,4] and numerical simulations.[5] When the Reynolds number is large but finite, vortex reconnection may take place, permitting a change of topology of the vortex lines. Individual events of such vortex reconnection have been studied, typically involving reconnection between isolated vortex tubes or rings.[6–11] Notably, in these simulations, the vortex tubes usually contort during their mutual approach, such that the vortex lines reconnect locally antiparallel (in a 2D plane). However, in many applications, the vorticity is a smooth nonvanishing function across the volume and cannot be modeled as a set of interacting isolated tubes. Examples include rotating stars and planets where there is a dominant direction of the vorticity (aligned with the rotation axis) onto which contributions from convection are superimposed. The resulting field could be interpreted as a vortex braid. If vortex reconnection occurs in such a scenario, the presence of a dominant unidirectional vorticity field means that the reconnection is fully three-dimensional,[12] as recently observed in the reconnection of vortex tubes with swirl.[9,13] Note that with "vortex reconnection" here we refer to the process by which the vorticity field lines change their topology, prohibited in a barotropic, inviscid fluid. This should not be confused with the notion of reconnection of vorticity isosurfaces, also sometimes referred to as vortex reconnection.

We analyze in the following the relaxation of a braided vorticity field in a fluid of high Reynolds number ($\mathrm{Re} > 10^4$). The aim is to investigate the extent to which the topology of the vorticity field—characterized by braided vorticity field lines—determines the dynamics. With the notion "braided," we describe a situation where we have a dominant component of the vorticity field in one direction, in our case the z-direction, so that all vorticity field lines connect two opposite sides of our domain (see Fig. 1). The motivation for this scenario is threefold: first, the situation of a braided vorticity field is of relevance for many cases of rotating astrophysical bodies, where the rotation of the star or planet provides a dominant component of the vorticity, and the contributions from convection or turbulence to the vorticity are weaker and only contribute to a braiding of the vortex lines. Second, this setup has the advantage that all vorticity lines connect from the lower to upper boundary of our domain. That is, there are no null points of the vorticity in the domain, and hence, the topological

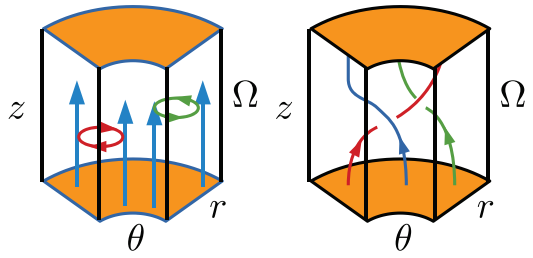

FIG. 1. Schematic representation of the initial setup of the vortex braid. Left, we represent the components of the field with the two vortex rings (red and green) of opposing vorticity sign and the background vorticity (blue). On the right, we show the superposition of the vortex rings with the background field which results in the vortex braid.

structure of the field is uniquely described by its vorticity-field line mapping from the lower to the upper boundary.[14] This allows us to analyze the topology of the field at any point in time using various tools such as the field line helicity,[14,15] the topological entropy,[16] or the topological degree.[17] With these tools, one can follow the dynamics of the relaxation with the ultimate aim to make predictions regarding the final state of the relaxation process. One can even identify individual processes of vortex reconnection taking place. However, in this study, we are less interested in the individual reconnection events and more in the collective effect that a turbulent cascade of reconnection events has on the route the relaxation process takes. The third motivation is that this vortex braid relaxation is the exact analogue to a magnetic braid relaxation studied by the authors before.[18] In these previous studies, the relaxation exhibited additional constraints on the dynamics, over and above the one imposed by the conservation of helicity.[17] To investigate the presence of such constraints in vortex dynamics is the aim of this study.

II. MODEL

A. Initial condition

We wish to construct a vortex braid in which all vorticity field lines connect between opposite boundaries of the domain. In order to facilitate direct comparison with a well-studied magnetic braid, we choose the particular braiding pattern of the vorticity lines to be analogous to that of the magnetic field lines in that magnetic braid.[18] The vorticity field consists of a constant background field in the z-direction together with two vortex rings with their symmetry axes also aligned to the z-direction. The vortex rings are located such that we obtain vorticity field lines as in Fig. 1 (see also Fig. 8). All vorticity lines connect between opposite (plane-parallel, constant-z) boundaries. The background vorticity field is conveniently obtained from a (solid-body) rotational flow with the z-axis as the axis of rotation. An illustration is shown in Fig. 1, which corresponds to the vortex field we will be using.

To avoid complications of generation of secondary vortices in domain corners, something that typically occurs in Cartesian geometries for rotating fluids, we make use of a cylindrical domain, which rotates about the z-axis. We construct the field first without the homogeneous background in a cylindrical wedge with periodic azimuthal boundaries and move the frame of reference together with the global rotational flow. To obtain the effect of the background field (and the full vortex braid), we add a Coriolis term in the momentum equations (see below).

Each of the vortex rings (red and green in Fig. 1) is constructed by first defining a single vortex ring centered at the origin. This greatly simplifies our calculations, due to the ring's azimuthal symmetry. We then translate the calculated field to its position in the wedge domain; a nontrivial transformation, as described in Appendix A.

For our computational domain, we choose a cylindrical wedge of dimensions $r \in [45, 65]$, $\theta \in [-0.1, 0.1]$, and $z \in [-16, 16]$. We choose the θ and z directions to be periodic, while the boundary conditions in the radial direction are chosen such that the normal component of the velocity vanishes and any mass flux is suppressed.

Within this domain, we place two vortex rings of opposite orientation, with axes lying in planes of constant z and centers at positions $(r,\theta,z) = (55, \arctan(1/55), -8)$ and $(r,\theta,z) = (55, -\arctan(1/55), 8)$. This means that the subsection of our volume in which the vortex lines exhibit a nontrivial tangling is located centrally within the domain, away from the r and θ boundaries. The initial vertical distance of 16 in. nondimensional code units between the (axes of the) vortex rings ensures that the velocities induced by the two vortex rings do not significantly overlap at $t=0$. Note that the superposition of the vortex ring with the background vorticity leads to a local twisting of the vorticity lines, and since the boundaries are periodic along z, the vorticity lines in principle pass through infinitely many of these vortex rings.

To prevent effects from supersonic flows, we choose the amplitude of the vorticity in the vortex rings to $\alpha = 0.1$. This will keep the velocities throughout the simulations well below the sound speed of 1. For the background vorticity, we choose $\boldsymbol{\Omega} = 0.1 e_z$. This will lead to a vorticity field with the desired topology. The ratio of the two amplitudes α/Ω determines the strength of the braiding and with that the topology of the vortex field. Note that this constant background vorticity refers to the rest frame and is achieved by using a Coriolis term in the simulations with the angular velocity $\tilde{\boldsymbol{\Omega}} = \boldsymbol{\Omega}/2$.

With these parameters, we obtain a Rossby number,

$$\mathrm{Ro} = \frac{u}{2L\tilde{\Omega}}, \tag{1}$$

where u is a typical velocity and L a typical length scale. In our case, $u \approx 0.1$ (velocity at the vortex rings), $L \approx 1$ (size of the vortex rings), and $\tilde{\Omega} = 0.05$. With that we have $\mathrm{Ro} \approx 1$.

B. Numerical setup

As described above, to circumvent issues at the domain's corners and issues with nonvanishing normal velocities at the boundaries, we place our cylindrical wedge domain in a comoving frame. This generates the additional term of the Coriolis force $2u \times \tilde{\boldsymbol{\Omega}}$. Our resulting equations are then the equations of motion for a viscous, isothermal, and compressible gas,

$$\frac{\mathrm{D}u}{\mathrm{D}t} = -c_s^2 \nabla \ln \rho + 2u \times \tilde{\boldsymbol{\Omega}} + F_{\mathrm{visc}}, \tag{2}$$

$$\frac{\mathrm{D}\ln\rho}{\mathrm{D}t} = -\nabla \cdot u, \tag{3}$$

with the isothermal speed of sound c_s, density ρ, viscous forces F_{visc}, and Lagrangian time derivative $\mathrm{D}/\mathrm{D}t = \partial/\partial t + u \cdot \nabla$. Here, the viscous forces are given as $F_{\mathrm{visc}} = \rho^{-1} \nabla \cdot 2\nu\rho S$, with the kinematic viscosity ν, and traceless rate of the strain tensor $S_{ij} = \frac{1}{2}(u_{i,j} + u_{j,i})$

$-\frac{1}{3}\delta_{ij}\nabla\cdot u$. Being an isothermal gas, we have $p = c_s^2\rho$ for the pressure. Note that since c_s^2 is constant, $\nabla p \times \nabla\rho = 0$, meaning that there is no baroclinic vorticity production.

Equations (2) and (3) are solved using the PencilCode,[19] which is an Eulerian finite-difference code using sixth-order spatial derivatives and a third-order time-stepping scheme.[20] Throughout our simulations, we use $\nu = 10^{-3}$ to $\nu = 4\times10^{-5}$ in order to reduce kinetic energy dissipation and kinetic helicity dissipation as much as the limited resolution of $512\times256\times256$ (r, θ, z) grid points allows. We emphasize that due to the barotropic nature of the fluid, in the inviscid case the tangling (or braiding) of the vortex lines would be preserved for all time.

C. Incompressibility

By construction, the initial velocity field has the property $\nabla\cdot u \approx 0$. Being approximately incompressible, any calculations involving the evolution of the kinetic energy or enstrophy significantly simplify. This implies that the initial uniform density does not change in time [see Eq. (3)]. However, numerical errors in the calculation of the potential C_0 [Eq. (A1)] can cause deviations from $\nabla\cdot u = 0$.

To check if our assumption of incompressibility holds true for all time, we plot the maximum and minimum densities in the domain as a function of time (Fig. 2). We observe a deviation of ca. 0.5% from the uniform density at the initial time, which quickly decreases to ca. 0.2% and approximately remains constant. Being such a small deviation, we can safely assume that the system is approximately incompressible.

III. EVOLUTION OF THE SYSTEM

Following initiation of the simulation, the two vortex rings travel toward one another due to their self-induced motion, meeting approximately at the mid-plane, $z=0$. This is analogous to the self-induced motion of an isolated infinitesimal vortex ring (i.e., with infinitesimal minor radius), with some distortion due to the presence of the background vorticity and the finite radius of the rings. Due to the offset in θ between the two rings, they do not meet face-on (Fig. 3). However, their collision leads to a local enhancement of the vorticity where they meet, as seen in the enstrophy evolution (see Sec. IV).

From previous studies of the relaxation of magnetic braids, we know that the braid constructed in this way requires many

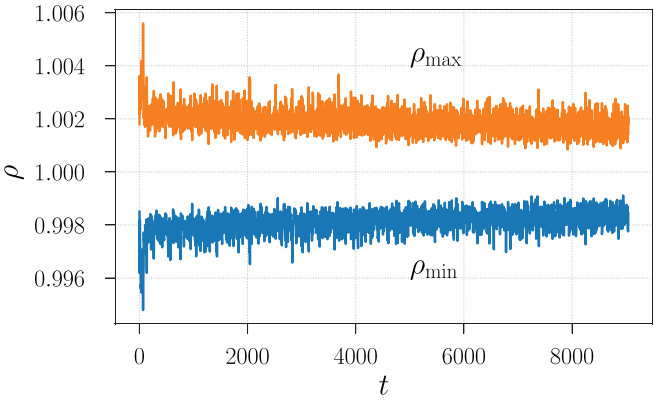

FIG. 2. Minimum and maximum densities in the domain as a function of time for the simulation with viscosity $\nu = 4\times10^{-5}$.

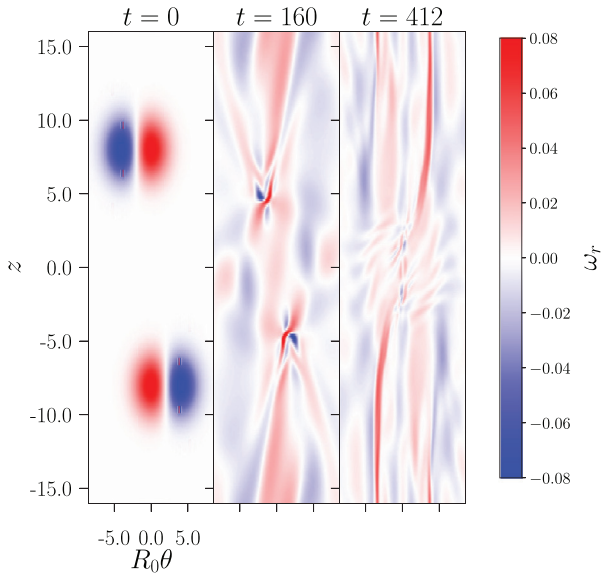

FIG. 3. Slices through the domain for ω_r at different times at $r = R_0 = 55$ for the simulation with viscosity $\nu = 4\times10^{-5}$.

reconnection events to untangle and is very efficient in generating a turbulent evolution. Following the initial collision, we see indeed that a highly fluctuating, "turbulent-like" evolution ensues, in which we find numerous locations at which vortex reconnection takes place (identified by calculating $(\nabla\times\omega)\cdot(\omega+\mathbf{\Omega})/|\omega+\mathbf{\Omega}|$, see Refs. 10 and 12) Through these many localized reconnection events, the field topology simplifies, with the vortex lines becoming less tangled. However, the final state retains a nontrivial topology, and our main purpose is to analyze the way in which this final state is determined by the initial field topology.

IV. ENSTROPHY

Unlike the total energy and the kinetic helicity, the enstrophy

$$\mathscr{E} = \int_V \omega^2\,\mathrm{d}V \tag{4}$$

is not necessarily conserved, even in the inviscid case. To see the factors that can lead to a change in enstrophy, we use the momentum Eq. (2) to write the vorticity equation as

$$\frac{\partial\omega}{\partial t} = m\nabla\times(u\times\omega) + 2\nabla\times(u\times\tilde{\mathbf{\Omega}}) + \nu\Delta\omega + 2\nu\nabla\times(\nabla\ln(\rho)\cdot S). \tag{5}$$

With this, we can write the time evolution of the total enstrophy as

$$\begin{aligned}\frac{\mathrm{d}\mathscr{E}}{\mathrm{d}t} &= 2\int_V \omega\cdot\frac{\partial\omega}{\partial t}\,\mathrm{d}V\\ &= 2\int_{\partial V}((u\cdot\omega)\omega + \nu\omega\times\nabla\times\omega)\cdot\mathrm{d}S\\ &\quad +2\int_V\big((u\times(\omega+2\tilde{\mathbf{\Omega}}))\cdot\nabla\times\omega - \nu(\nabla\times\omega)^2\\ &\quad +2\nu\omega\cdot\nabla\times(\nabla\ln(\rho)\cdot S)\big)\,\mathrm{d}V,\end{aligned} \tag{6}$$

where we used the fact that the azimuthal and vertical dimensions are periodic, $u \cdot n = 0$ at the r boundaries and $\tilde{\mathbf{\Omega}} \cdot n = 0$ on the r and θ boundaries.

Apart from the terms involving viscosity, we have two more volume terms and one surface term that in general do not vanish. This is interesting, since our domain is closed in the radial direction and yet, there can be enstrophy fluxes through those boundaries. However, throughout all of our simulations, the velocities near the radial boundaries are very small and this term can be safely ignored. The first volume term describes the dynamical generation or annihilation of enstrophy according to the alignment of the velocity, vorticity, and its curl, while the second volume term describes the dynamical generation/annihilation of enstrophy due to the Coriolis force.

For high Reynolds numbers, we observe first an increase and then a gradual decrease in enstrophy (Fig. 4). As the vortex rings approach and collide, a large amount of vorticity is produced on small scales. Since this is a turbulent effect, it increases as we increase the Reynolds number. Indeed, the breakup of vortex sheets formed during vortex tube/ring collision is well-documented.[9,21,22] For higher Reynolds numbers, the flow becomes more turbulent and the nonviscous terms in Eq. (6) become more dominant. It appears that the alignment of the fields is such that a net production of enstrophy is obtained. In numerical vortex reconnection, experiments[23,24] showed a similar behavior of enstrophy production during reconnection events. With increasing Reynolds number, they too observe an increased enstrophy production. The Coriolis contribution to the enstrophy evolution seems to dampen the production through the term $(u \times \omega) \cdot \nabla \times \omega$.

V. KINETIC HELICITY

In the inviscid case, the kinetic helicity (hereafter, simply "helicity") is conserved. For a nonvanishing viscosity, this will not be the case anymore. However, for the present configuration, due to the symmetry of the configuration, consisting of a vortex ring with positive helicity and one with negative helicity, the volume-integrated helicity is zero and stays zero at all times. Nevertheless, the existence of helicity in parts of the domain can influence relaxation. Indeed, it has been shown that in the relaxation of magnetic braids, not only the net helicity is important in constraining the dynamics but also properties of the field line mapping as well as the helicity-per-fieldline spectrum.[17,25,26] A way to detect the existence of a nonvanishing helicity density in the domain is to track the evolution of the unsigned kinetic helicity as the integral over the magnitude of the helicity density,

$$\bar{H}_{\mathrm{kin}} = \int_V |(\omega + \mathbf{\Omega}) \cdot (u + U)| \, \mathrm{d}V, \tag{7}$$

where $\nabla \times U = \mathbf{\Omega}$. Note that here we include the background vorticity and velocity; that is, we calculate the helicity in an inertial frame rather than the corotating frame. This is for two reasons. First, helicity conservation holds for the inertial frame but not in general for an accelerated frame. Second, only in the inertial frame do we have properly braided vorticity lines in the initial state, while in the corotating frame, the kinetic helicity density vanishes everywhere at $t = 0$.

Furthermore, one has to note that unsigned kinetic helicity is not conserved, even under conditions where the usual kinetic helicity is conserved. For instance, if an initially straight untwisted vortex tube fixed between two parallel plates is deformed by a rotation in the middle, then the helicity is conserved as the left- and right-hand twists in the tube cancel, but the unsigned helicity increases. Nevertheless, the unsigned helicity is always positive and can vanish only if the helicity density vanishes everywhere in the domain. The latter property is important for what follows, as it captures any nonzero helicity density in the domain.

We have run our simulations for different values of Re, and it is instructive to plot the results using time units that are normalized by the viscous dissipation timescale,

$$\tau \approx L^2/\nu, \tag{8}$$

where L is a typical length. Here we take L to be the (major) radius of the vortex rings which is approximately 1.

For our simulations, we observe first a steep rise of $\bar{H}_{\mathrm{kin}}$ and then dissipation. Since for $\nu = 10^{-3}$, we have $\tau = 1000$ this means that by time 1000 we should observe a significant decrease in kinetic helicity. Indeed, at time $t/\tau = 0.5$, we observe a drop by a factor of $e^{-0.5}$ compared to its peak value at early times (Fig. 5).

The initial rise happens at approximately 100 code time units, independent of the viscosity, which means that it is a nonviscous effect. As the two initial vortex rings approach, we observe an increase in kinetic helicity density until the time of collision, which is approximately 100 code time units. This we attribute to vortex stretching. After that, we observe that the viscosity takes over and dissipates $\bar{H}_{\mathrm{kin}}$. Note that for $\nu = 10^{-3}$, 100 code time units corresponds to $t/\tau = 0.1$, while for $\nu = 10^{-4}$, the collision time is $t/\tau = 0.01$ in normalized times.

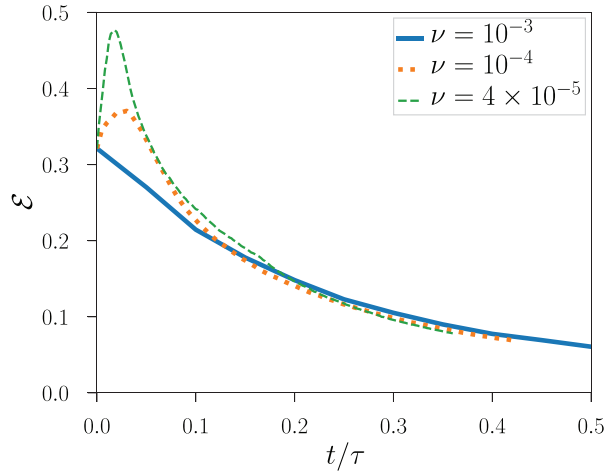

FIG. 4. Enstrophy evolution for different viscosities ν against normalized (diffusion) time [see Eq. (8)].

A. Kinetic helicity and enstrophy

The motivation to consider the relation between helicity and enstrophy comes from the magnetic case where we know that the magnetic energy is limited from below by the magnetic helicity. This is known as the realizability condition,[27–30]

$$|H_{\mathrm{mag}}| \leq \frac{2}{\lambda} E_{\mathrm{mag}}, \tag{9}$$

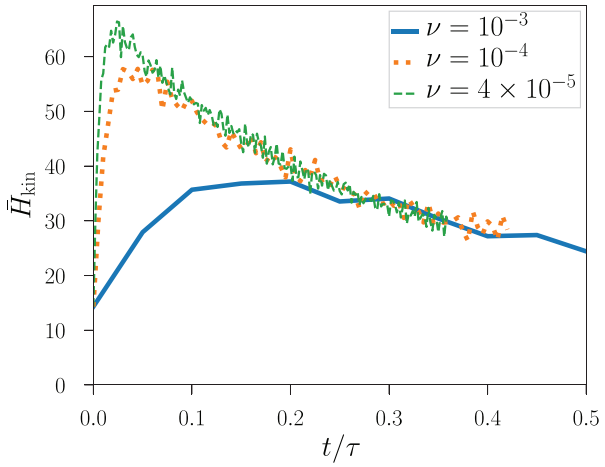

FIG. 5. Evolution of the unsigned kinetic helicity for the relaxing vortex braid for different viscosities ν against normalized time [see Eq. (8)].

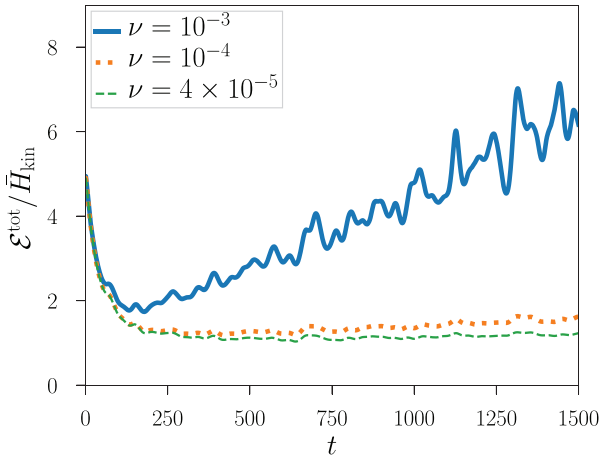

FIG. 6. Evolution of the ratio of enstrophy with unsigned kinetic helicity for different viscosities ν against simulation time.

where λ is the smallest positive eigenvalue of the curl operator in the domain.[27,31] The inequality is sharp; that is, there exist fields for which the equality holds and these are the eigenfields of the curl operator for the minimal eigenvalue $\pm\lambda$. The corresponding condition for vorticity fields would involve the enstrophy in the rest frame $\mathcal{E}^{\mathrm{tot}}$ and not the energy,

$$|H_{\mathrm{kin}}| \leq \frac{1}{\lambda}\mathcal{E}^{\mathrm{tot}}. \tag{10}$$

Since the helicity is defined in the rest frame, we also have to use the definition of the enstrophy in the rest frame,

$$\mathcal{E}^{\mathrm{tot}} = \int_V (\omega + \mathbf{\Omega})^2 \, \mathrm{d}V. \tag{11}$$

In our case, this inequality is not very useful since $H = 0$, which does not pose any lower bound on the enstrophy. However, as shown in Appendix B, we can find an even stronger inequality,

$$\bar{H}_{\mathrm{kin}} \leq \frac{1}{\lambda}\mathcal{E}^{\mathrm{tot}}, \tag{12}$$

$$\Longleftrightarrow \lambda \leq \frac{\mathcal{E}^{\mathrm{tot}}}{\bar{H}_{\mathrm{kin}}}. \tag{13}$$

The minimal λ is not easy to determine for our domain, but one can approximate by using the known minimal $\lambda = (2.405..)/R$ for a cylinder. The largest cylinder we can fit into our domain has $R = 5$; hence, the λ for our domain should be roughly 0.48. The ratio $\mathcal{E}^{\mathrm{tot}}/\bar{H}_{\mathrm{kin}}$ is shown in Fig. 6 and we clearly see that the enstrophy is bounded from below by the unsigned kinetic helicity with a ratio ≥ 1.

For the curve with the highest viscosity, we find after the initial relaxation an increase in the ratio $\mathcal{E}^{\mathrm{tot}}/\bar{H}_{\mathrm{kin}}$. This is a result of our particular setup. As the viscous dissipation does not act on the fixed background vorticity field, the evolution will eventually dissipate everything but the background field and for the latter the ratio $\mathcal{E}^{\mathrm{tot}}/\bar{H}_{\mathrm{kin}}$ is infinite. Hence after the first dynamic relaxation, the ratio will eventually increase again also for the other two curves.

B. Kinetic helicity and kinetic energy

Next, we study the relation between the integrated kinetic helicity and kinetic energy. In order to be consistent with the helicity calculation, we need to calculate the energy also in the rest frame, with velocity $u + U$ and vorticity $\omega + \mathbf{\Omega}$. With a much larger U compared to u (since $|U| \propto r \in [45, 65]$), the energy would be dominated by the background velocity. So in order to prevent that any change is obscured by the large background contribution, we compute the "free" kinetic energy instead; that is, we subtract the energy of the background field,

$$E_{\mathrm{kin}}^{\mathrm{free}} = \int_V \rho\left(\frac{1}{2}u^2 + u \cdot U\right) r \, \mathrm{d}r \, \mathrm{d}\theta \, \mathrm{d}z. \tag{14}$$

Due to the Coriolis force, inertial waves are induced whose dominant frequency is determined by the background rotation rate. Combined with a background velocity U that is large compared to u, we see large periodic fluctuations of $E_{\mathrm{kin}}^{\mathrm{free}}$. Therefore, to reveal the limiting behavior, we compute running means for our values $E_{\mathrm{kin}}^{\mathrm{free}}/\bar{H}_{\mathrm{kin}}$ over 100 time units.

Although a strict lower limit for the kinetic energy is not known, we observe that the ratio of the free kinetic energy and unsigned kinetic helicity tends asymptotically to a nonzero value (Fig. 7) with the limit value of ca. 0.0025. This is so striking that it leads us to conclude that there exists a lower limit for kinetic energy in the presence of unsigned kinetic helicity.

This finding is complementary to previous findings on helical turbulent flows in rotating frames[32,33] where the authors studied the effect of net kinetic helicity and rotation on the kinetic energy decay. They find that, while helicity in a nonrotating frame does not affect the energy decay, in a rotating frame, helicity poses restrictions leading to a slower decay.

VI. FIELD TOPOLOGY

Our simulated configuration consists of two vortex rings. However, we aim to compare our results to previous works using three pairs of such vortex rings (e.g., Wilmot-Smith *et al.*[18]) Therefore, for

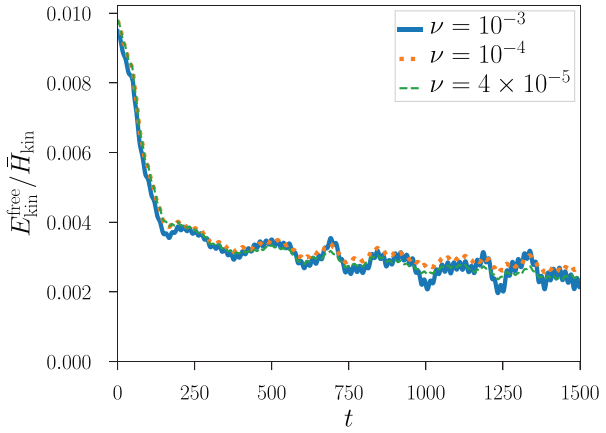

FIG. 7. Evolution of the ratio of free kinetic energy with unsigned kinetic helicity for different viscosities ν against simulation time. Here, we use a running mean with a window of 100 time units to smooth out oscillatory behavior induced by inertial waves.

the discussion in this section, we will make use of the periodicity in the z-direction and construct such a braid by following vortex streamlines over three periods.

A. Simplification of the topology

In order to analyze the changing topology of the vorticity field, we integrate—at each instant of time—a set of vorticity field lines starting from a fixed grid of starting points on the lower boundary ($z = -16$). Naively, we would expect the vortex field to simplify into a homogeneous field in the z-direction (due to the net-zero helicity, this should be the lowest-energy state). However, as time progresses, and the field lines reconnect due to the finite viscosity, the topology of the field simplifies (Fig. 8) not to an untwisted field, but—similar to the magnetic case[17,25]—into two large-scale vorticity tubes containing twisted vortex lines, of opposite twist (swirl). The fact that this final state mirrors closely the final state of the relaxation of a magnetic braid in a plasma (with the same initial topology) suggests that some unifying underlying conservation principle is shared between the two systems.

B. Field line helicity

The above-mentioned simplification of the topology is effectively quantified/visualized by plotting the *kinetic field line helicity*, constructed as follows. Due to the positive z-component of the vorticity, any field line starting at the lower domain boundary will end at the top boundary. This way we can find a one-to-one mapping between the boundaries. For that, we trace 256^2 field lines starting at the lower boundary that are equally spaced in the radial direction $r \in [49, 60]$ and the azimuthal direction $\theta \in [-0.1, 0.1]$. We use those field lines to compute the kinetic field line helicity,

$$\mathscr{A}(x_0, y_0) = \int_C \frac{((u+U)(x,y,z) \cdot (\omega(x,y,z) + \mathbf{\Omega})}{(\omega(x,y,z) + \mathbf{\Omega})_z} \, \mathrm{d}z, \qquad (15)$$

where $x(x_0, y_0, z)$ and $y(x_0, y_0, z)$ are the mapped points along the vorticity field line paths, C.[15] This measures the amount of winding[34]

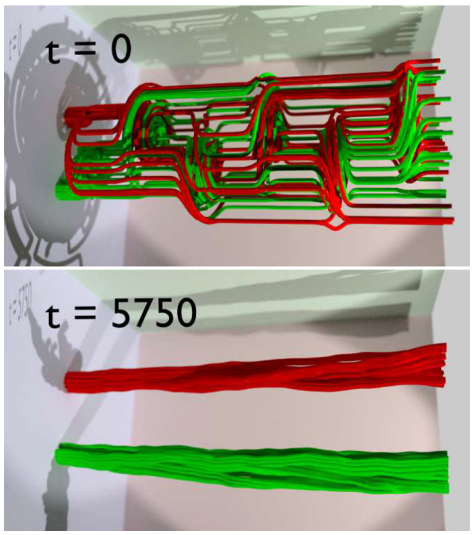

FIG. 8. Vortex streamlines in the rest frame (with background vorticity) for the $\nu = 4 \times 10^{-5}$ case at time $t = 0$ (upper panel) and $t = 5750$ (lower panel). In order to compare with previous simulations of magnetic braids, we repeat our computational domain in the z-direction (horizontal in these plots) three times. The initial braid is largely unbraided and the final configuration consists of two separated vortex tubes of opposite twist.

of each field line around all other field lines and gives us a picture about the distribution of the helicity even in cases where its net value vanishes.

Since our vortex braid is highly tangled, the distribution of the field line helicity at initial time shows some complexity at relatively small scales (Fig. 9, upper panel). As time progresses and the field lines reconnect, the distribution simplifies greatly into two separate regions with opposite-field line helicity (Fig. 9, lower panel), which corresponds to the two flux tubes of opposite twist/swirl described above.

Indeed, Ref. 15 showed that there is a connection between the reconnection rate and the source term of the field line helicity, which for the hydrodynamic case takes the form

$$\frac{\mathrm{D}\mathscr{A}}{\mathrm{D}t} = -\nu \int_C \frac{\nabla \times \omega \cdot (\omega + \mathbf{\Omega})}{|(\omega + \mathbf{\Omega})|} \, \mathrm{d}l, \qquad (16)$$

where l is the arc length along the vorticity line C.

VII. CONCLUSIONS

We performed simulations of the relaxation of nonhelical vortex braids in a cylindrical wedge domain for a viscous fluid. While the kinetic energy viscously decays, we observe an increase in the integrated norm of the kinetic helicity density at dynamical times. This increase is due to the reconnection of the vortex field lines at early times and coincides with the time the flux rings that generate the braid collide.

The most striking finding of our study is that the unsigned kinetic helicity appears to constrain the relaxation of the studied vortex braid. Specifically, the ratio of the kinetic energy to unsigned helicity approaches a nonzero value at late times that is independent of the viscosity. This implies the presence of additional topological constraints

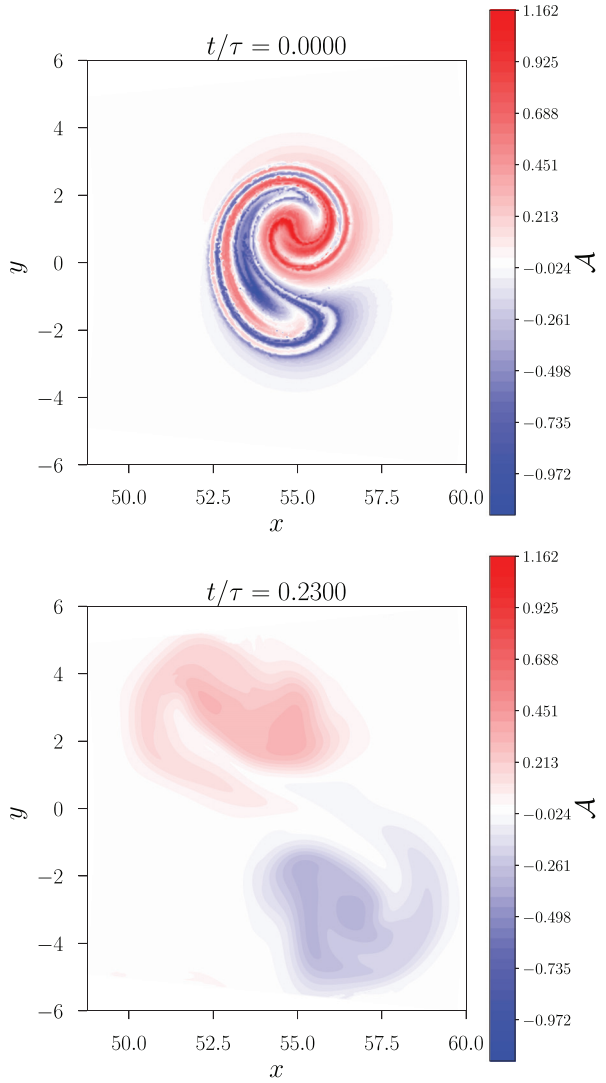

FIG. 9. Field line helicity distribution in the rest frame (with background vorticity) of the vortex field at initial time (upper panel) and normalized time $t/\tau = 0.230$ (lower panel), which corresponds to $t = 5750$ [see Eq. (8)], for the run with $\nu = 4 \times 10^{-5}$. In order to compare with previous simulations of magnetic braids, we repeat our computational domain in the z-direction three times. Here, we use $x = r\cos(\theta)$ and $y = r\sin(\theta)$ for the coordinates.

on the hydrodynamic relaxation process that may be related to those discovered recently for the magnetohydrodynamic system. In magnetohydrodynamics, it is known that the presence of magnetic helicity imposes a lower bound for the magnetic energy. At the same time, we know from numerical experiments that topologically nontrivial magnetic braids are not free to decay, even in the case of net-zero magnetic helicity. The presence of additional topological constraints, such as preservation of the fixed point index or the field line helicity, restricts the field's decay.[17,26,35] For the hydrodynamic case, such relations between the kinetic energy and kinetic helicity are not known, but the present results strongly suggest their existence.

However, for the enstrophy, we derived a lower bound in the presence of unsigned kinetic helicity. This relation is similar to the magnetohydrodynamic case, but with the enstrophy replacing the energy. Our simulations clearly confirm the validity of this analytical result and we suggest that this relation should be taken into account when studying the relaxation of hydrodynamical systems.

In addition to the above, we discovered another close parallel between the final states of our vortex braid relaxation and magnetic braid relaxations. Specifically, for the same braid topology, the two cases relax toward a topologically equivalent final state, as revealed by plotting, e.g., the field line helicity (Fig. 9). The fact that the final states of these two very different relaxation processes are analogous for the braid considered suggests that the constraints are likely also related to one another, and the exploration of these topological constraints in the hydrodynamic system will be an important area of future study.

ACKNOWLEDGMENTS

S.C., D.I.P., and G.H. acknowledge financial support from the UK's STFC (Grant Nos. ST/N000714/1 and ST/S000267/1). For the plots, we made use of the Matplotlib library for Python[36] and BlenDaViz.[37]

APPENDIX A: CONSTRUCTION OF VORTEX TUBES

In our simulations, the variables that are solved for are not the vorticity ω, but the velocity u. So, we need to specify our initial conditions in terms of u with $\nabla \times u = \omega$. Yet, for a given vorticity ω, we can find different velocities u such that $\nabla \times u = \omega$, similar to the gauge freedom for the magnetic vector potential A with the magnetic field $\boldsymbol{B} = \nabla \times A$. However, it is not desirable to use the expression for the vector potential from Wilmot-Smith *et al.*[18] for our velocity field u as it is not divergence-free, leading to unwanted compression.

In order to construct a divergence-free flow field, we use the solutions of the Biot–Savart integral for a singular vortex ring (see Jackson,[38] Sec. 5.5). We then construct the vortex ring from a sum (integral) of infinitely many infinitesimally thin vortex rings. For that, we compute a potential C such that $u = \alpha\nabla \times (Ce_\theta)$ which results in a divergence-free velocity field by construction.

We first construct the potential C_0 for a single vortex ring in a coordinate system with origin at the ring's center. In a later step, we will shift (transform) this potential to its actual position. Our coordinates here are (r_0, θ_0, z_0). Here, the potential $C_0(r_0, \theta_0, z_0)$ is the double integral,

$$C_0(r_0, \theta_0, z_0) = \int_{-8}^{8} \mathrm{d}z_0' \int_0^5 \mathrm{d}r_0' \sqrt{2} r_0' e^{-r_0'^2/2 - z_0'^2/4} \Psi, \tag{A1}$$

with

$$\Psi = \frac{r_0'\left((\kappa^2+2)K(\kappa) - 2E(\kappa)\right)}{\pi\sqrt{r_0'^2 + r_0^2 + (z_0 - z_0')^2 + 2r_0' r_0}\,\kappa^2}, \tag{A2}$$

with the complete elliptical integral of the first kind $K(\kappa)$, complete elliptical integral $E(\kappa)$, and

$$\kappa = 2\sqrt{\frac{r_0' r_0}{r_0'^2 + r_0^2 + (z_0 - z_0')^2 + 2r_0' r_0}}. \tag{A3}$$

We choose to integrate in z_0' from -8 to 8 and in r_0' from 0 to 5; as beyond those integration intervals, the integrand is sufficiently small to be neglected from the integration. For more details about this construction, see the study of Jackson in Ref. 38, Sec. 5.5.

This gives us the vector potential $C_0(r_0, \theta_0, z_0)\mathbf{e}_{\theta_0}$ in the centered coordinate system (r_0, θ_0, z_0). In order to construct the braid, we make a coordinate transformation so that our ring is centered at $r = R_0, \theta = \Theta$. The coordinates transform according to

$$r_0 = \sqrt{r^2 + R_0^2 - 2rR_0\cos(\theta - \Theta)}, \tag{A4}$$

$$\theta_0 = \arctan(\sin(\theta - \Theta)/\cos(\theta - \Theta) - R_0/r), \tag{A5}$$

$$z_0 = z, \tag{A6}$$

while the vector potential transforms as

$$C_r(r, \theta, z) = \frac{-C_0(r_0, \theta_0, z_0)R_0\sin(\theta - \Theta)}{\sqrt{-2R_0r\cos(\theta - \Theta) + R_0^2 + r^2}}, \tag{A7}$$

$$C_\theta(r, \theta, z) = \frac{C_0(r_0, \theta_0, z_0)(r - R_0\cos(\theta - \Theta))}{\sqrt{-2R_0r\cos(\theta - \Theta) + R_0^2 + r^2}}. \tag{A8}$$

After this transformation, we apply the curl operator in the wedge domain and obtain the initial velocity in the wedge domain. The resulting vortex rings have a minor and major radius of ca. 1.

APPENDIX B: INEQUALITY FOR THE UNSIGNED HELICITY

The relation between unsigned kinetic helicity and enstrophy is derived using the Poincaré inequality,

$$\left(\int_V ||u||^2\,\mathrm{d}^3x\right)^{1/2} \le \frac{1}{\lambda}\left(\int_V ||\omega||^2\,\mathrm{d}^3x\right)^{1/2}, \tag{B1}$$

which holds for every differentiable field, such that $\omega = \nabla \times u$. Here λ is the smallest positive eigenvalue of the curl operator.

We can now apply the Cauchy–Schwarz inequality to the unsigned kinetic helicity density to obtain

$$\int_V |\omega \cdot u|\,\mathrm{d}^3x \le \int_V ||\omega||||u||\,\mathrm{d}^3x, \tag{B2}$$

and apply it a second time to the integral (L^2-norm version),

$$\int_V |\omega \cdot u|\,\mathrm{d}^3x \le \left(\int_V ||\omega||^2\,\mathrm{d}^3x\right)^{1/2}\left(\int_V ||u||^2\,\mathrm{d}^3x\right)^{1/2}. \tag{B3}$$

Eventually, we use the Poincaré inequality to obtain

$$\int_V |\omega \cdot u|\,\mathrm{d}^3x \le \frac{1}{\lambda}\int_V ||\omega||^2\,\mathrm{d}^3x. \tag{B4}$$

This leaves us with the inequality,

$$\bar{H}_{\mathrm{kin}} \le \frac{1}{\lambda}\mathscr{E}. \tag{B5}$$

DATA AVAILABILITY

Raw data were generated using HPC facilities. Derived data supporting the findings of this study are available from the corresponding author upon reasonable request.

REFERENCES

[1]H. K. Moffatt, "The degree of knottedness of tangled vortex lines," J. Fluid Mech. **35**, 117–129 (1969).
[2]H. K. Moffatt, "Relaxation under topological constraints," in *Topological Aspects of the Dynamics of Fluids and Plasmas*, edited by H. K. Moffatt, G. M. Zaslavsky, P. Comte, and M. Tabor (Springer, Dordrecht, The Netherlands, 1992), pp. 3–28.
[3]M. W. Scheeler, D. Kleckner, D. Proment, G. L. Kindlmann, and W. T. M. Irvine, "Helicity conservation by flow across scales in reconnecting vortex links and knots," Proc. Natl. Acad. Sci. U. S. A. **111**, 15350–15355 (2014).
[4]M. W. Scheeler, W. M. van Rees, H. Kedia, D. Kleckner, and W. T. M. Irvine, "Complete measurement of helicity and its dynamics in vortex tubes," Science **357**, 487–491 (2017).
[5]R. M. Kerr, "Topology of interacting coiled vortex rings," J. Fluid Mech. **854**, R2 (2018).
[6]W. T. Ashurst and D. I. Meiron, "Numerical study of vortex reconnection," Phys. Rev. Lett. **58**, 1632–1635 (1987).
[7]M. V. Melander and F. Hussain, "Cross-linking of two antiparallel vortex tubes," Phys. Fluids **1**, 633–636 (1989).
[8]S. Kida, M. Takaoka, and F. Hussain, "Collision of two vortex rings," J. Fluid Mech. **230**, 583–646 (1991).
[9]W. M. van Rees, F. Hussain, and P. Koumoutsakos, "Vortex tube reconnection at $\mathrm{Re} = 10^4$," Phys. Fluids **24**, 075105 (2012).
[10]P. McGavin and D. I. Pontin, "Vortex line topology during vortex tube reconnection," Phys. Rev. Fluids **3**, 054701 (2018).
[11]X. Zhao, Z. Yu, J.-B. Chapelier, and C. Scalo, "Direct numerical and large-eddy simulation of trefoil knotted vortices," J. Fluid Mech. **910**, A31 (2021).
[12]G. Hornig, "The Geometry of Reconnection," *An Introduction to the Geometry and Topology of Fluid Flows*, edited by R. L. Ricca (Kluwer, 2001).
[13]P. McGavin and D. I. Pontin, "Reconnection of vortex tubes with axial flow," Phys. Rev. Fluids **4**, 024701 (2019).
[14]A. R. Yeates and G. Hornig, "Unique topological characterization of braided magnetic fields," Phys. Plasmas **20**, 012102 (2013).
[15]A. R. Yeates and G. Hornig, "A generalized flux function for three-dimensional magnetic reconnection," Phys. Plasmas **18**, 102118 (2011).
[16]S. Candelaresi, D. I. Pontin, and G. Hornig, "Quantifying the tangling of trajectories using the topological entropy," Chaos **27**, 093102 (2017).
[17]A. R. Yeates, G. Hornig, and A. L. Wilmot-Smith, "Topological constraints on magnetic relaxation," Phys. Rev. Lett. **105**, 085002 (2010).
[18]A. L. Wilmot-Smith, G. Hornig, and D. I. Pontin, "Magnetic braiding and parallel electric fields," Astrophys. J. **696**, 1339 (2009).
[19]See Github.com/pencil-code/ for the latest version of the Pencil Code.
[20]A. Brandenburg and W. Dobler, "Hydromagnetic turbulence in computer simulations," Comput. Phys. Commun. **147**, 471–475 (2002).
[21]R. M. Kerr, "Fully developed hydrodynamic turbulence from a chain reaction of reconnection events," Procedia IUTAM **9**, 57–68 (2013).
[22]R. McKeown, R. Ostilla-Mónico, A. Pumir, M. P. Brenner, and S. M. Rubinstein, "Cascade leading to the emergence of small structures in vortex ring collisions," Phys. Rev. Fluids **3**, 124702 (2018).
[23]J. Yao and F. Hussain, "A physical model of turbulence cascade via vortex reconnection sequence and avalanche," J. Fluid Mech. **883**, A51 (2020).
[24]V. L. Nguyen and V. D. Duong, "Vortex ring-tube reconnection in a viscous fluid," Phys. Fluids **33**, 015122 (2021).
[25]D. I. Pontin, A. L. Wilmot-Smith, G. Hornig, and K. Galsgaard, "Dynamics of braided coronal loops. II. Cascade to multiple small-scale reconnection events," Astron. Astrophys. **525**, A57 (2011).
[26]A. R. Yeates, A. J. B. Russell, and G. Hornig, "Physical role of topological constraints in localized magnetic relaxation," Proc. R. Soc. A **471**, 20150012 (2015).
[27]V. I. Arnold, "The asymptotic Hopf invariant and its applications," Sel. Math. Sov. **5**, 327 (1986).
[28]A. Brandenburg, W. Dobler, and K. Subramanian, "Magnetic helicity in stellar dynamos: New numerical experiments," Astron. Nachr. **323**, 99–122 (2002).
[29]F. Del Sordo, S. Candelaresi, and A. Brandenburg, "Magnetic-field decay of three interlocked flux rings with zero linking number," Phys. Rev. E **81**, 036401 (2010).

[30]S. Candelaresi and A. Brandenburg, "Decay of helical and nonhelical magnetic knots," Phys. Rev. E **84**, 016406 (2011).
[31]V. Arnold and B. Khesin, *Topological Methods in Hydrodynamics* (Springer, New York, 2013).
[32]T. Teitelbaum and P. D. Mininni, "The decay of turbulence in rotating flows," Phys. Fluids **23**, 065105 (2011).
[33]T. Teitelbaum and P. D. Mininni, "Effect of helicity and rotation on the free decay of turbulent flows," Phys. Rev. Lett. **103**, 014501 (2009).
[34]M. A. Berger, "An energy formula for nonlinear force-free magnetic fields," Astron. Astrophys. **201**, 355–361 (1988).
[35]A. R. Yeates and G. Hornig, "Dynamical constraints from field line topology in magnetic flux tubes," J. Phys. A **44**, 265501 (2011).
[36]J. D. Hunter, "Matplotlib: A 2d graphics environment," Comput. Sci. Eng. **9**, 90–95 (2007).
[37]See Github.com/SimonCan/BlenDaViz for the latest version of BlenDaViz.
[38]J. Jackson, *Classical Electrodynamics*, 3rd ed. (Wiley India Pvt. Limited, 2007), Chap. 5.5.